Title
Cellulose nanofibrils improve dispersibility and stability of silver nanoparticles and induce production of bacterial extracellular polysaccharides

Journal
Journal of Materials Chemistry B, 2(37)

ISSN
2050-750X

Authors
Wang, Min S
Jiang, Feng
Hsieh, You-Lo
et al.

Publication Date
2014-10-07

DOI
10.1039/c4tb00630e

Peer reviewed

Journal of Materials Chemistry B

PAPER

View Article Online
View Journal | View Issue

Cite this: J. Mater. Chem. B, 2014, 2, 6226

Cellulose nanofibrils improve dispersibility and stability of silver nanoparticles and induce production of bacterial extracellular polysaccharides†

Min S. Wang,[a] Feng Jiang,[b] You-Lo Hsieh[b] and Nitin Nitin*[ac]

Received 22nd April 2014
Accepted 17th July 2014

DOI: 10.1039/c4tb00630e

www.rsc.org/MaterialsB

Many polymer-stabilized silver nanoparticles (AgNPs) with enhanced antibacterial properties have been synthesized, but very little is known about the fate of these materials and their interactions with microbes in physiological solutions. In this study, we evaluated the role of cellulose nanofibrils (CNFs) in stabilizing AgNPs (CNF–AgNPs) in a bacterial growth medium, determined the antibacterial properties of CNF–AgNPs and assessed the CNF and CNF–AgNP interactions with bacteria. The attachment of AgNPs to CNFs significantly improved the stability and dispersibility of AgNPs in the bacterial growth medium compared to colloidal AgNPs. The CNF–AgNPs exerted a concentration-dependent growth-inhibitory effect on *E. coli*. An extracellular polysaccharide (EPS)-like structure was formed around the *E. coli* bacterium when incubated with a sub-lethal CNF–AgNP concentration, which led to the clustering of neighboring bacteria. No EPS-like structure was observed around the bacterium incubated with high concentration of CNF–AgNPs. Overall, this study demonstrated that CNFs significantly improved the stability and dispersibility of AgNPs in physiological medium, validated the antimicrobial potential of CNF–AgNPs, and provided an insight into the physio-chemical interactions between bacteria and CNF–AgNPs in a physiological growth medium.

Introduction

Colloidal silver nanoparticles (AgNPs) have long been known to possess antibacterial and bacteriostatic (growth inhibiting) properties,[1–4] but they are prone to aggregation in physiological solutions.[5–7] Aggregated AgNPs in physiological solutions can limit their use as antibacterial agents, as previous studies have suggested that smaller AgNP colloids possess greater antibacterial activity and lower minimum inhibitory concentration compared to larger AgNP aggregates.[4,8,9] To limit aggregation of AgNPs in physiological media, various polymers such as chitosan,[10] starch,[11] nanofibrillated cellulose,[12,13] cellulose nanocrystals,[14–20] as well as bacterial cellulose[1,5,21] have been utilized to stabilize AgNPs.

Polymer stabilized AgNPs have been used for many diverse applications including antimicrobial surfaces and materials. While many studies have evaluated the antibacterial properties of these polymer-stabilized AgNPs,[1,5,22–24] very little is known about the fate of these polymer-stabilized AgNPs in physiological solutions, or the resulting microbial–material interactions in suspension. It has been suggested that both physical and chemical properties of AgNPs (*e.g.*, shape, size, surface charge),[4,8,9] as well as the physio-chemical interactions between AgNPs and physiological solutions[25] can influence the fate and antibacterial properties of AgNPs. Moreover, since polymers such as chitosan and the PEI are known to possess antibacterial properties on their own, it is difficult to distinguish the antibacterial effects from the AgNPs *versus* the polymeric stabilizing material. Therefore, this study was aimed at: (1) characterizing the stability and dispersibility of cellulose nanofibril stabilized AgNPs (CNF–AgNPs) in a bacterial growth medium, (2) evaluating the dynamic interaction between the nanomaterial and bacteria in suspension, and (3) quantifying the bacterial response to the CNF and CNF–AgNPs.

Rice straw-derived cellulose nanofibrils (CNFs) were selected as the stabilizing polymer because they are by-products of rice cultivation and provides a sustainable source to create functional nanomaterials with enhanced chemical and mechanical properties such as well-defined size and surface morphology,[12,16–18] in

[a]Food Science and Technology Department, University of California Davis, Davis, CA 95616, USA. E-mail: nnitin@ucdavis.edu

[b]Fiber and Polymer Science, University of California Davis, Davis, CA 95616, USA

[c]Department of Biological and Agricultural Engineering, University of California Davis, Davis, CA 95616, USA

† Electronic supplementary information (ESI) available: Dispersibility and stability of CNF–AgNPs after dialysis and over time, effects of free Ag^+ and unbound AgNPs on bacterial growth, fluorescence images showing live/dead bacteria using PI and Sybr Green staining, and the TEM image showing clustering of multiple bacteria caused by CNF–AgNPs. See DOI: 10.1039/c4tb00630e

addition to having a high aspect ratio and surface charge density. Because of its large surface area to volume ratio, and ease of surface modification, cellulose nanostructures have been used to stabilize AgNPs for DNA detection,[18] to improve the mechanical and antimicrobial properties of polyurethane films,[19] or as a template to attach metallic nanoparticles.[13,16,17,20]

CNFs derived from 2,2,6,6-tetramethylpiperidine-1-oxyl (TEMPO) mediated oxidation of rice straw cellulose with the most surface C6 hydroxyls converted to carboxyls were selected for their maximal surface charge effect in this study.[28,30] CNF–AgNPs were synthesized by reducing silver ions (Ag^+) with borohydride (BH_4^-) in the presence of CNFs as the capping agent. Electrostatic binding of Ag^+ to CNF surface carboxyls and the subsequent reduction of Ag^+ to atomic silver (Ag^0) and AgNPs were monitored using Fourier transformed infrared spectroscopy (FTIR) and energy-dispersive X-ray spectroscopy (EDS). The synthesized CNF–AgNPs were characterized by ultraviolet-visible (UV-vis) spectroscopy, atomic force microscopy (AFM) and transmission electron microscopy (TEM). The stability of CNF–AgNPs in a growth medium was evaluated using UV-vis spectroscopy and compared with that of colloidal AgNPs. The influence of CNFs and CNF–AgNPs on bacterial activity was determined based on the changes in bacterial growth rate, metabolic activity, and viability. Structural changes of the bacteria, CNFs and CNF–AgNPs as a result of interactions between bacteria and these materials were further characterized using optical microscopy and TEM.

The findings of this study highlighted the properties of CNFs for improving the stability and dispersibility of AgNPs in a physiological growth medium, and the unique interactions between bacteria and CNF–AgNPs. Overall, the results of this study provide an improved understanding of the interactions between bacteria and polymer-stabilized AgNPs, and will have profound impact on the design of antibacterial materials.

Materials and methods

Materials

Pure cellulose was isolated from rice straw (Calrose variety, harvested in northern California in 2009).[26] *E. coli* BL21 and MTT assay kit (30-1010K) were from ATCC, Manassas, VA. Phosphate buffered saline (PBS), LB agar miller, and LB broth were from Fisher Scientific, Waltham, MA. SYBR Green DNA label was from Invitrogen (Carlsbad, CA). All other chemicals were from Sigma-Aldrich (St. Louis, MO) and used as received unless otherwise specified.

Synthesis of CNF

Pure cellulose was isolated from rice straw by extraction with 2 : 1 v/v toluene–ethanol. The extracted material was subsequently treated with acidified sodium chlorite for 5 h ($NaClO_2$, 1.4%, 70 °C), followed by potassium hydroxide for 2 h (KOH, 5%, 90 °C) to remove lignin and hemicellulose/silica, respectively.[26,27] Cellulose nanofibrils (CNFs) were defibrillated from pure rice straw cellulose *via* 2,2,6,6-tetramethylpiperidine-1-oxyl (TEMPO) mediated oxidation (10 mmol g^{-1} of NaClO) followed by mechanical blending (37 000 rpm, 25 min).[28]

Synthesis of CNF–AgNPs and colloidal AgNPs

CNF–AgNPs were synthesized by reducing silver nitrate ($AgNO_3$) with sodium borohydride ($NaBH_4$) in the presence of 0.1 wt% CNFs as the capping agent. Typically, 0.6 mL of 50 mM $AgNO_3$ was added to 7.9 mL CNF suspension for 5 min, then 1.5 mL of 100 mM ice-cooled $NaBH_4$ was added to react for 30 min to make 10 mL of 0.1 wt% CNF–AgNP solution. The solution was dialyzed (nominal MWCO, 3500) against deionized (DI) water for 3 h to remove unbound Ag^+ and BH_4^- as well as unattached AgNPs. The retentate was diluted to 20 mL with DI water. To evaluate the Ag^+ binding with CNFs, CNF–Ag was prepared by adding 0.6 mL of 50 mM $AgNO_3$ to 9.4 mL of CNF suspension at the same $AgNO_3$: CNF ratio as above and mixed for 5 min, then dialyzed for 3 h to remove free Ag^+.

Colloidal AgNPs were synthesized according to the standard borohydride reduction method with slight modifications.[29] Briefly, 100 mL of aqueous 10 mM $NaBH_4$ was stirred continuously in an ice bath and kept at 4 °C throughout the synthesis. Then, 1 mL of 100 mM $AgNO_3$ was added drop-wise (1 mM $AgNO_3$ final concentration) under constant stirring in an ice bath until a pale yellow solution was observed, indicating the formation of colloidal AgNPs. The colloidal AgNPs were kept in the dark at 4 °C until use.

Concentrations of AgNPs on CNF–AgNPs by UV-vis spectroscopy

The concentrations of AgNPs on CNF–AgNPs were quantified by UV-vis spectroscopy (Evolution 600, Thermo Scientific). To obtain a standard calibration curve, AgNPs synthesized on CNFs prior to dialysis (3 mM Ag^+) were serially diluted to 0.01–0.175 mM of equivalent Ag^+ concentrations. The concentrations of AgNPs were evaluated at three time intervals, *i.e.*, immediately upon synthesis, post-dialysis and after 5 months of refrigerated storage.

Size distribution of AgNPs by TEM

To determine the size of AgNPs on the CNF–AgNP sample, a drop (10 μL) of CNF–AgNP suspension (1 : 100 dilution) was deposited on a glow-discharged carbon coated TEM grid 300-mesh copper, formvar-carbon (Ted Pella Inc., Redding, CA) and air-dried. The samples were observed using a Philip CM12 transmission electron microscope operated at a 100 kV accelerating voltage. The particle size of AgNPs on CNF–AgNPs was determined from the TEM images and analyzed using ImageJ (http://rsbweb.nih.gov/ij/).

Surface topography of CNF–AgNPs characterized by atomic force microscopy (AFM)

The CNF and CNF–AgNPs were imaged by AFM (Asylum-Research MFP-3D, Santa Barbara, CA) using tapping mode with OMCL-AC160TS standard silicon probes. Each sample was prepared by depositing 10 μL CNF–AgNP suspension containing 0.0001 wt% CNFs onto a freshly cleaved mica surface, air-dried and scanned at 1 Hz and 512 × 512 pixels resolution. The topographic images and height profiles were processed with the Igor Pro 6.21 software (MFP3D 090909 + 1409). The height and

length of CNFs and AgNPs were determined from *ca.* 100 individual nanoparticles.

Chemical composition of CNF–AgNPs characterized by Fourier transformed infrared (FTIR) and energy-dispersive X-ray spectroscopy (EDS)

Chemical composition of both CNF–Ag and CNF–AgNPs were investigated using FTIR and EDS. The CNF, CNF–Ag and CNF–AgNP suspensions (20 mL, 0.05 wt% CNFs) were freeze-dried (FreeZone 1.0L Benchtop Freeze Dry System, Labconco, Kansas City, MO) and the FTIR spectra of freeze-dried samples in KBr pellets (1 : 100, w/w) were collected under ambient conditions using a Thermo Nicolet 6700 spectrometer. The spectra were collected in the transmittance mode from an accumulation of 128 scans at a 2 cm^{-1} resolution over the 4000–400 cm^{-1} regions. The elemental compositions of dialyzed and freeze-dried CNF, CNF–Ag and CNF–AgNPs were measured using the EDS (X-Max^N Silicon Drift Detector, Oxford Instruments, Abingdon, Oxfordshire, England) adjunct to the SEM at a magnification of 500× with a 12 kV accelerating voltage and a 5 mm working distance. All elemental compositions were reported in atomic percentage.

Stability of CNF–AgNPs and colloidal AgNPs in LB media

The stability of CNF–AgNPs and colloidal AgNPs in LB media was determined using UV-vis spectroscopy. CNF–AgNPs and colloidal AgNPs were diluted with LB media (150 μM of equivalent Ag^+ concentration) in a 15 mL tube and incubated at 37 °C under constant agitation at 250 rpm. One milliliter of solution from each tube was sampled and analyzed at 0 min, and every hour for 6 hours. The absorbance spectra were recorded from 350–900 nm with a 5 nm resolution using a Thermo Scientific Genesys 10UV spectrophotometer (Thermo-Fisher Scientific, Waltham, MA).

Bacterial culture and growth assay

E. coli BL21 was used as a model Gram-negative bacterium. Fresh bacterial cultures were obtained by picking one colony from the LB agar plate and incubated overnight in LB growth media at 37 °C. A 1 : 100 dilution of this overnight culture was used for the growth assay. To test the effects of CNF–AgNPs on bacterial growth, CNFs (0.008%) and CNF–AgNPs (150 and 450 μM of equivalent Ag^+) were diluted in LB media, and 200 μL of each CNF or CNF–AgNP solution was pipetted into a 96-well plate. To each well, 2 μL of *E. coli* BL21 suspension (10^7 CFU per mL) was added to each well and the bacterial growth kinetics were monitored by optical density (OD) measurement using a SpectraMax 340 microplate reader (Molecular Devices). The absorbance at 600 nm (OD_{600}) was taken every 5 min, and the plate was shaken for 5 s prior to each measurement. The bacterial growth kinetics were measured for 18 h at 37 °C.

Cell viability by tetrazolium (MTT) reduction assay

To access cell viability, stationary phase *E. coli* BL21 (10^7 CFU per mL) was incubated with CNFs (0.008%) and CNF–AgNPs (150 and 450 μM of equivalent Ag^+) and control in LB media in a 96-well plate for 18 h at 37 °C. After 18 h, 25 μL of the (3-(4,5-dimethylthiazol-2-yl)-2,5-diphenyltetrazolium bromide) MTT substrate was added to each sample and incubated for 3 h at 37 °C in the dark. Viable cells with active dehydrogenase enzymes will reduce the MTT from a yellow solution to insoluble purple formazan crystals. Then, 100 μL DMSO was added to each well to solubilize the formazan crystals. After 10 min of incubation at 37 °C in the dark, the absorbance was measured at 560 nm and normalized to the control.

Plate count assay

The number of viable bacterial cells after incubation with CNFs (0.008%) and CNF–AgNPs (150 and 450 μM of equivalent Ag^+) was enumerated using the standard plate count assay. Briefly, bacterial cells from each well were serially diluted with sterile water and spread uniformly on a LB agar plate. The LB agar plates were incubated overnight at 37 °C and bacterial cell colonies were counted the following day.

Quantification silver using inductively coupled plasma atomic emission spectroscopy (ICP-AES)

To measure the changes in Ag^+ concentration in the CNF–AgNPs (150 μM of Ag^+ equivalent concentration) after incubation with LB media, the total silver content of the CNF–AgNP sample was quantified using ICP-AES (Thermo iCAP6500) at a wavelength of 328.068 nm, and compared to the control (CNF–AgNP in water). Following an 18 h of incubation under constant agitation on a shaker/incubator at 250 rpm at 37 °C, the CNF–AgNP samples were centrifuged at 5000 rpm for 5 min to pellet large CNF–AgNP aggregates. The pellet was re-suspended with water, and both the supernatant and the pellet for each sample were digested using nitric acid and analyzed separately for their total silver concentration.

Fluorescence microscopy analysis of the bacterial suspension after incubation with CNFs and CNF–AgNPs

Following 18 h of incubation with CNFs (0.008%) and CNF–AgNPs (150 and 450 μM of equivalent Ag^+) at 37 °C, the changes to bacterial suspension in the bulk solution were characterized by fluorescence microscopy. The bacteria in each sample were labelled using a DNA intercalating dye (SYBR Green) for 5 min at room temperature, and the fluorescence microscopy images of the samples were taken using an Olympus IX-71 inverted fluorescence microscope with a 10× objective (Olympus UPlanFLN). The excitation and emission settings for the microscope were 480/30 nm and 535/40 nm, respectively.

Structural analysis of bacteria by TEM

Changes in the morphology of bacterial cells after incubation with CNFs and CNF–AgNPs were observed by TEM. A 8 μL sample (1 : 100 dilution) was placed on a carbon coated TEM grid (400 mesh, Ted Pella, Redding, CA) and incubated for 10 min. The excess solution was removed using a filter paper, and 8 μL of 1% ammonium molybdate was added to negatively stain

the sample. The stain was quickly wicked away and the TEM grid was allowed to dry in air for 10 min prior to imaging. The samples were viewed using a Philips CM120 Biotwin TEM (FEI Company, Hillsboro, OR, USA) operated at 80 kV and TEM images were acquired using the Gatan TEM Imaging software.

Statistical analysis

All experiments were repeated 3 times and the data were presented as mean ± SD. A p-value of <0.05 is considered as statistically significant based on Student's t-test.

Results and discussion

Synthesis of CNF–AgNPs

CNFs obtained after TEMPO mediated oxidation of pure rice straw cellulose were 2.0 (±0.7) nm in diameter, hundreds to thousands of nanometer in length and were highly crystalline (CrI = 84.8%).[30] The TEMPO mediated oxidation regioselectively converts over 93% surface C6 primary hydroxyls of CNFs to carboxyls and produces negatively charged CNFs.[30] Upon $AgNO_3$ addition, Ag^+ ions were electrostatically attached to negatively charged carboxyls on CNF surfaces, and Ag^+ was subsequently reduced to AgNPs by $NaBH_4$ (Fig. 1A). The excess Ag^+ and BH_4^-, as well as unattached AgNPs were removed by dialysis and analyzed by FTIR and EDS. The FTIR spectrum of CNFs showed a broad peak at 1616.1 cm^{-1} and a small peak at 1722.1 cm^{-1}, assigned to asymmetrical stretching of sodium carboxylate (COO^- Na^+) and carboxylic carbonyl (C=O), respectively (Fig. 1B). Upon addition of $AgNO_3$ into CNFs, the COO^- Na^+ peak shifted to 1610.3 cm^{-1}, indicating the replacement of Na^+ with Ag^+. The C=O peak at 1722.1 cm^{-1} remained unchanged, indicating the non-participating role of COOH groups in Ag^+ binding as expected. This is consistent with previous findings that showed the minimum adsorption of Ag^+ onto carboxylate sites when all the carboxyls are protonated.[31] Upon the reduction of Ag^+ to AgNPs by $NaBH_4$, the C=O stretching peak at 1722.1 cm^{-1} disappeared and the asymmetrical stretching vibration of the COO^- Na^+ peak shifted slightly back to 1612.2 cm^{-1} (Fig. 1B). The disappearance of the 1722.1 cm^{-1} peak suggested the ionization of COOH by $NaBH_4$ to COO^- Na^+, while the peak shift observed at 1612.2 cm^{-1} was from the overlapping stretching vibrations of both COO^- Na^+ (1613.1 cm^{-1}) and carboxylates coordinated with AgNPs.

The EDS analysis of the CNF sample showed the characteristic C, O and Na peaks at 0.27, 0.52, and 1.04 keV, respectively (Table 1), with a Na atomic concentration of 3.2%. For the

Table 1 Atomic concentration of Na and Ag in CNFs, CNF–Ag and CNF–AgNPs

	Atomic concentration (%)	
Samples	Na	Ag
CNFs	3.2 ± 0.3	0
CNF–Ag	1.4 ± 0.3	1.2 ± 0.1
CNF–AgNPs	3.5 ± 0.2	8.7 ± 0.4

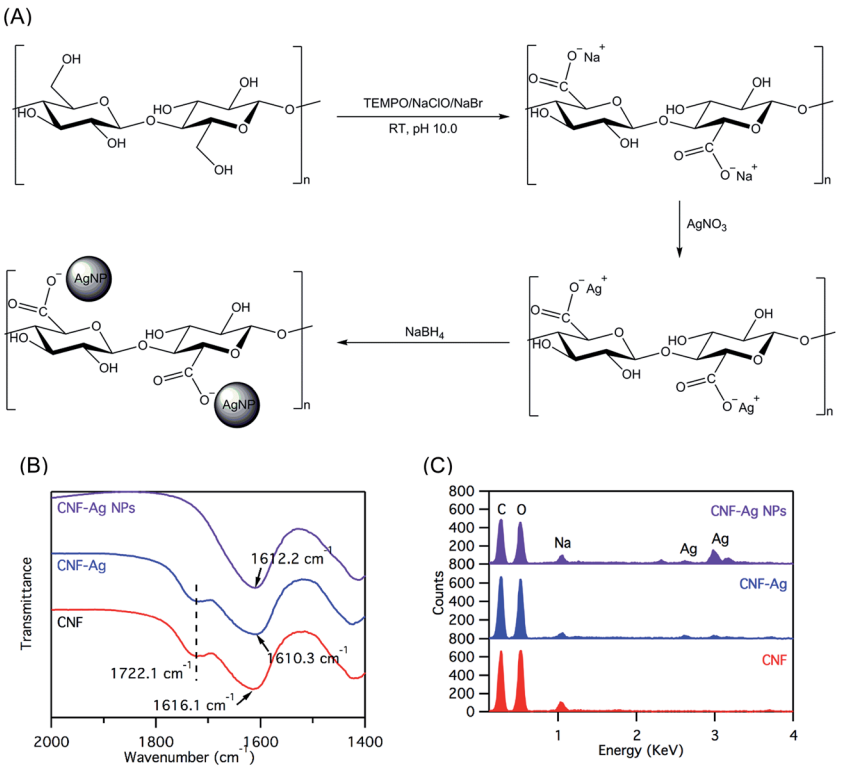

Fig. 1 (A) Schematic illustration depicting the attachment of Ag^+ ions to CNFs, and the subsequent reduction of Ag^+ to AgNP with $NaBH_4$. (B) FTIR and (C) EDS spectra of CNFs (red), CNF–Ag (blue) and CNF–AgNPs (purple).

CNF–Ag samples, the EDS showed atomic Ag peaks at 2.61, 2.98 and 3.16 keV. Based on this analysis, the total Ag atomic concentration was 1.2% (Table 1). The Na atomic concentration of the CNF–Ag samples was reduced to 1.4%, consistent with the partial replacement of Na^+ with Ag^+ as indicated by FTIR (Fig. 1B). Upon reduction with $NaBH_4$, the Ag atomic concentration of CNF–AgNPs increased to 8.7%, indicating the growth of AgNPs on CNFs (Fig. 1C). The Na atomic concentration of the CNF–AgNP sample also increased from 3.2 to 3.5% (Table 1), indicating the conversion of COOH to COO^- Na^+ as shown by FTIR (Fig. 1B). Thus, both FTIR and EDS analyses supported the initial replacement of Na^+ with Ag^+ and subsequent reduction of Ag^+ to AgNPs upon addition of $NaBH_4$ (Fig. 1A–C and Table 1).

To further confirm the removal of free Ag^+ and BH_4^-, as well as unattached AgNPs by dialysis, the pre- and post-dialysis samples were analyzed and compared. The UV-vis spectra of the pre-dialyzed sample (Fig. 2A) showed a relatively narrow (full-width half maximum, FWHM = 62 nm) and symmetrical surface plasmon resonance (SPR) peak with a maximum absorbance wavelength (λ_{max}) of 397 nm, suggesting that the AgNPs were spherical and smaller than 20 nm in diameter.[32] After dialysis, CNF–AgNPs showed a golden yellowish color similar to the pre-dialyzed sample (inset, Fig. 2A), and the λ_{max} remained at 396 nm (Fig. 2A). However, the maximum absorbance (A_{max}) of the dialyzed CNF–AgNPs was lower and the peak shape was slightly broader (FWHM = 79 nm), compared to the pre-dialyzed sample (Fig. 2A, gray line). The reduced absorbance reflected the removal of AgNPs after dialysis and the slight peak shape broadening could be ascribed to the removal of small and unbound AgNPs, as well as the increased polydispersity of the AgNPs bound to CNFs. A standard calibration curve (A_{max} *vs.* equivalent Ag^+ concentration) was generated with equivalent Ag^+ concentration ranging from 0.01–0.175 mM based on the UV-vis spectra of pre-dialyzed samples (Fig. 2B). From this standard calibration curve, the equivalent Ag^+ concentration on CNF–AgNPs was determined to be 0.93 ± 0.01 mM, which corresponded to a 62% retention of AgNPs following dialysis. The dialyzed CNF–AgNPs showed no signs of aggregation and remained stable after 5 months of refrigerated storage as indicated by the minimal peak shift and A_{max} decrease (ESI, Fig. S1A†).

The TEM image of the dialyzed CNF–AgNPs (Fig. 2C) showed that AgNPs had an average diameter of 6.3 ± 3.1 nm (Fig. 2D). AFM images of CNF–AgNPs revealed that the CNFs were 1–2 nm thick with variable lengths (100–1000 nm) (Fig. 3A and C), and AgNPs had diameters ranging from 2–20 nm (Fig. 3B and D). The UV-vis data together with TEM and AFM imaging showed that the CNF bound AgNPs were larger than those removed during dialysis, and their sizes remained unchanged after 5 months of refrigerated storage (ESI, Fig. S1†). In addition, the UV-vis data also suggested that 38% of the AgNPs were unbound to the CNF and were removed during dialysis.

Dispersibility and stability of AgNPs in complex media

The dispersibility and stability of CNF–AgNPs in LB media were compared to those of colloidal AgNPs using UV-vis spectroscopy. CNF–AgNPs and colloidal AgNPs (both at 150 μM equivalent Ag^+ concentration) were dispersed in LB media and the

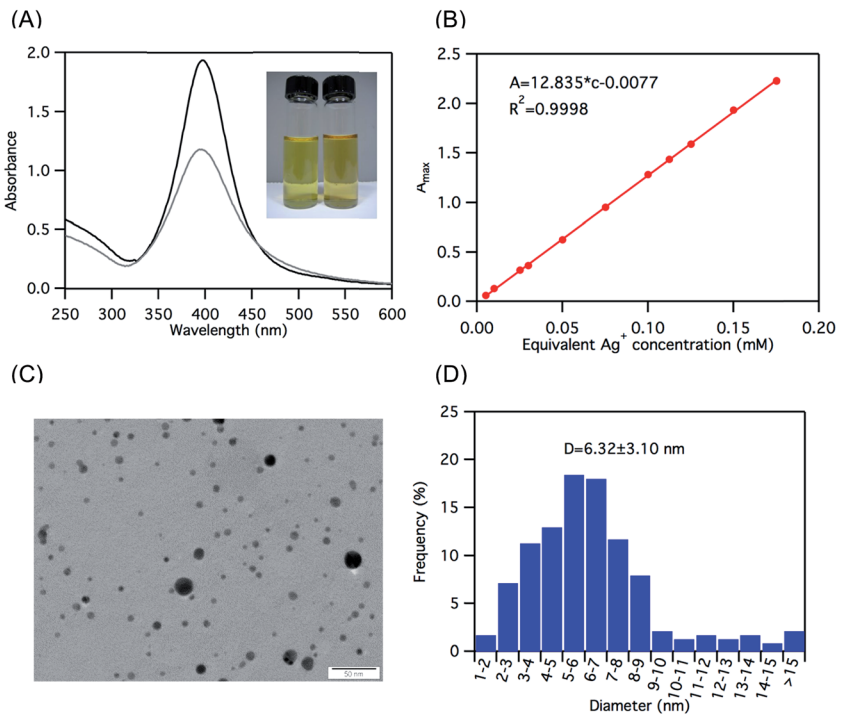

Fig. 2 (A) UV-vis absorbance spectra of CNF–AgNPs (black, pre-dialysis; gray, post-dialysis) inset: photographs of CNF–AgNPs before (left) and after (right) dialysis. (B) A standard calibration curve from a serial dilution of the pre-dialyzed CNF–AgNPs. (C) TEM images and (D) size distribution of post-dialyzed CNF–AgNPs from approximately 200 nanoparticles. Scale bar = 50 nm.

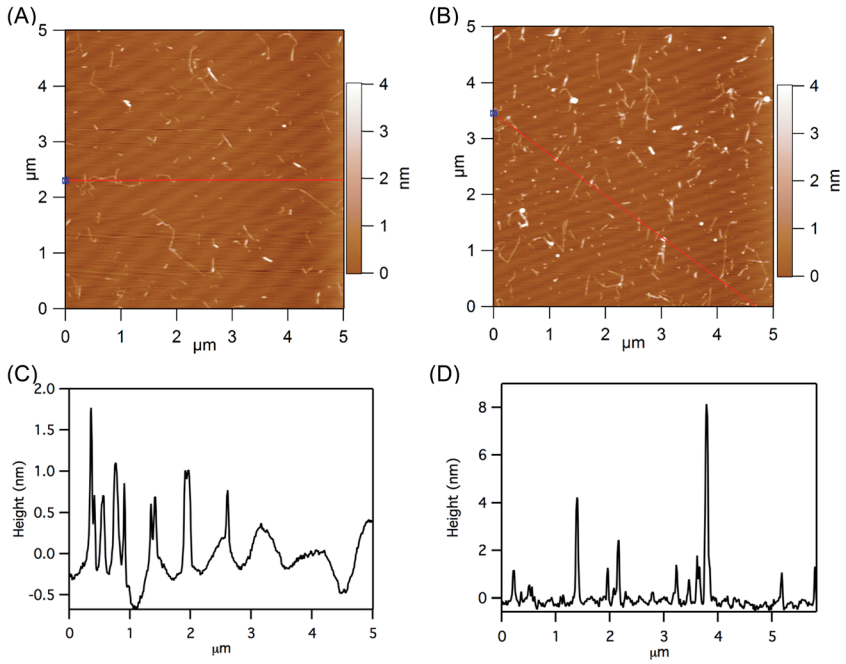

Fig. 3 (A and B) AFM height images and (C and D) profiles of the CNF and CNF–AgNPs.

UV-vis spectra were acquired every hour for 6 hours (Fig. 4). The colloidal AgNPs diluted with water showed two distinct λ_{max} at 390 nm and 480 nm (Fig. 4A), indicating that the colloidal AgNPs diluted in water were polydisperse. When the colloidal AgNPs were diluted with LB media, broad peaks with λ_{max} at 415 nm and 515 nm were observed at 0 h, indicating immediate aggregation of colloidal AgNPs (Fig. 4A). After 1 h, the changes to the UV-vis spectrum (*i.e.*, peak broadening, right shift in λ_{max}, and decrease in A_{max}) were clear indications that the colloidal AgNPs in LB media were mostly aggregated (Fig. 4A). No significant changes to the UV-vis spectrum were observed during 6 h of incubation of colloidal AgNPs in LB media after the initial measurement at 0 h (Fig. 4A).

On the other hand, the UV-vis spectrum of CNF–AgNPs in water showed only one λ_{max} at 390 nm (Fig. 4). Upon dilution with LB media, the λ_{max} shifted to 405 nm with slight peak broadening (FWHM = 120 nm) at 0 h (Fig. 4B). At 1 h, the λ_{max} shifted to 420 nm, and the FWHM of the peak increased to 155 nm (Fig. 4B). After 2 h of incubation, the λ_{max} remained at 420 nm, but the FWHM of the SPR peak increased to 170 nm (Fig. 4B). The results from the UV-vis spectroscopy suggested that AgNPs bound to CNFs could be dispersed in a complex solution, such as LB media, with slight aggregation of AgNPs after the initial hour of incubation (Fig. 4B). This is in contrast to colloidal AgNPs that aggregated within minutes when dispersed in LB media, and proceeded to precipitate from the LB media in 1 h (Fig. 4A). To further demonstrate the dispersibility and stability of CNF–AgNPs in LB media after 18 h at 37 °C, the CNF–AgNP sample was centrifuged to separate the pellet and supernatant fractions, and the total silver content was analyzed by ICP-AES (Table 2). Based on the ICP-AES analysis, the total silver content of CNF–AgNPs in the control (water)

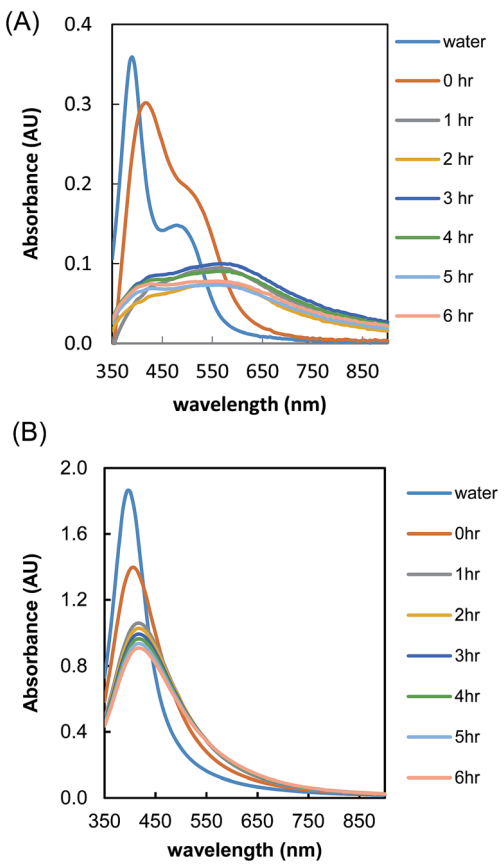

Fig. 4 UV-vis absorbance spectrum of (A) borohydride capped colloidal AgNPs and (B) CNF–AgNPs diluted in LB media at 37 °C over a period of 6 h.

Table 2 ICP-AES analysis of the total silver content of the CNF–AgNP after incubation in LB media. The CNF–AgNP was incubated in water (control) or LB media for 18 h at 37 °C. The supernatant and pellet were separated by centrifugation and analyzed independently. Data represent mean ± SD, $N = 3$

Sample	Silver (mg L^{-1})	Silver (μM)
CNF–AgNPs in water	20.6 ± 0.4	191.0 ± 4.0
CNF–AgNPs in LB media	19.8 ± 1.5	183.6 ± 13.8

and in the supernatant of the LB media was 191 ± 4 μM and 184 ± 14 μM, respectively (Table 2). This corresponded to a 96% retention of total silver in the LB media compared to the control. No silver could be quantified in the pellet fraction of both the water control and the CNF–AgNP in LB media, suggesting that most of the AgNPs remained bound to the CNFs and were dispersible in either water or LB media. The slight increase in Ag^+ concentration (from a starting CNF–AgNP concentration of 150 μM) was likely due to evaporation of water during overnight incubation at 37 °C.

The size and shape of the CNF–AgNPs and colloidal AgNPs dispersed in LB media (both at 150 μM equivalent Ag^+ concentration) were further determined by TEM. The average diameter of the AgNPs on CNF–AgNPs and colloidal AgNPs prior to the dispersion in LB media was 6 nm and 20 nm, respectively (Fig. 5A and B). It was also shown in the TEM image (Fig. 5A) that most of the AgNPs were attached to the CNFs, which was consistent with the AFM observation (Fig. 3B). Following an overnight incubation in LB media, the AgNPs remained attached to CNFs and were 7 nm in diameter, except for a few larger (~20 nm) particles (Fig. 5C). In contrast, large AgNP aggregates (over 1 μm) were observed in the colloidal AgNP sample (Fig. 5D). The significant degree of aggregation of colloidal AgNPs compared to the CNF suggested that CNFs were excellent dispersant of AgNPs in LB media, consistent with UV-vis measurements (Fig. 4).

Overall, the results of the stability analysis showed that the fate of CNF–AgNPs and AgNPs was influenced by the surrounding environment (water *vs.* bacterial growth medium). Both the UV-vis and imaging analyses demonstrated that CNF bound AgNPs had better dispersibility and stability in LB media compared to colloidal AgNPs. As suggested in a prior study, the stability and dispersion of AgNPs in aqueous suspension could be improved *via* steric repulsion of the surface adsorbed polymers, or through the electrostatic screening of the disperse phase to prevent the interaction between nanoparticles.[33] Therefore, the high aspect ratio and the surface charge on CNFs could provide steric hindrance and charge screening to reduce inter-particle interactions and coalescence.

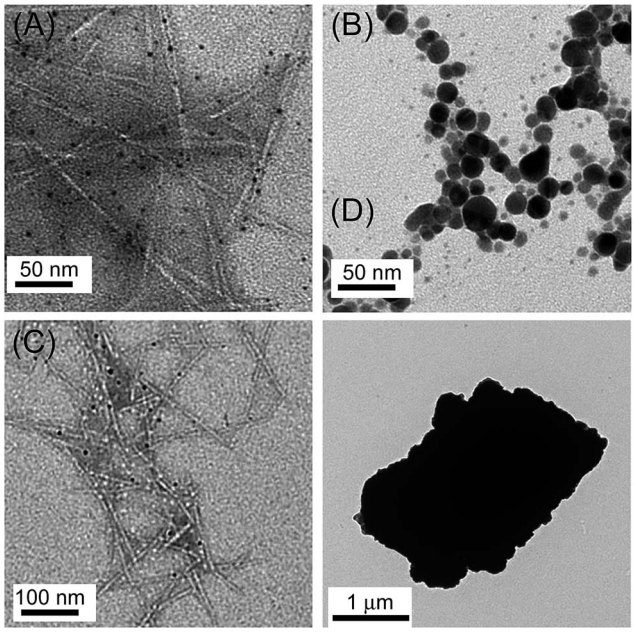

Fig. 5 TEM images of CNF–AgNPs and colloidal AgNPs. (A) CNF–AgNPs and (B) borohydride-capped colloidal AgNPs diluted in water. (C) CNF–AgNPs and (D) colloidal AgNPs after 18 h of incubation in LB media at 37 °C.

CNF–AgNPs reduce bacterial growth and viability

The effects of CNF–AgNPs on the growth and viability of *E. coli* bacteria were monitored by an overnight incubation of bacteria with CNFs or CNF–AgNPs. In the presence of CNFs, the bacteria followed a similar growth curve as the control sample, showing no effect of CNFs on *E. coli* growth (Fig. 6). On the other hand, incubation of bacteria with CNF–AgNPs resulted in a concentration-dependent growth inhibition (Fig. 6). When incubated with 150 μM CNF–AgNPs, a longer lag phase (1.5 h) was observed compared to the control (45 min), and bacterial growth plateaued at $OD_{600} = 0.27$ (Fig. 6). However, incubation of *E. coli* with 450 μM CNF–AgNPs resulted in a growth-inhibition compared to the control or the 150 μM CNF–AgNP (Fig. 6).

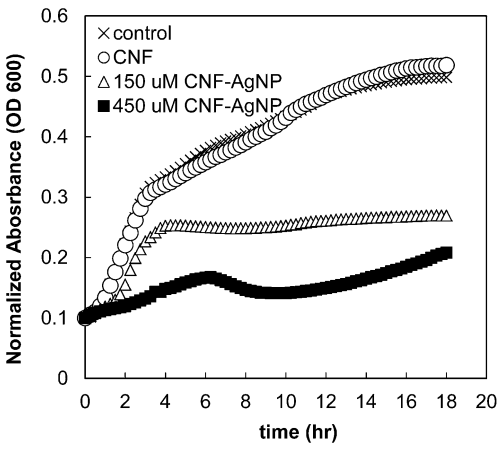

Fig. 6 Inhibition of bacterial growth. CNFs (○) and CNF–AgNPs (150 μM, Δ; 450 μM, ■) were incubated with *E. coli* BL21 and grown for 18 h at 37 °C. A control sample (×) without any added CNFs or CNF–AgNPs was incubated under the same conditions. The optical density was measured at 600 nm at 5 min interval for 18 h.

The bacterial cell viability was subsequently evaluated using the MTT assay and standard plate counting (Table 3). The MTT assay showed that the cell viability was similar for the CNF and 150 μM CNF–AgNPs compared to the control (Table 3). However, a 40% reduction in cell viability was observed when *E. coli* was incubated with 450 μM CNF–AgNPs (Table 3). The plate count assay further confirmed that CNFs alone did not affect cell viability; however, the 150 and 450 μM CNF–AgNPs caused a 1 and 3 log CFU decrease in bacterial counts, respectively, compared to the control (Table 3). The discrepancy between the MTT assay and plate counting results could be due to the range of sensitivity of the MTT assay, as well as the cytotoxicity of the formazan crystals compared to the standard plate counting.

The bacterial inhibitory concentration of CNF–AgNPs used in this study was noticeably higher than those reported for colloidal AgNPs[3,24] and non-dialyzed cellulose nanocrystal-stabilized AgNPs.[14] One key difference in the CNF–AgNPs evaluated in this study as compared to colloidal AgNPs and cellulose stabilized AgNPs is the level of free Ag^+ and smaller unbound AgNPs in the samples. Using a dialysis process, the results of this study indicated a significant reduction in the concentration of unbound AgNPs and free Ag^+ ions (Fig. 2). To evaluate the influence of unbound AgNPs and/or free Ag^+ on antibacterial properties, we compared the growth of bacteria incubated with dialyzed and non-dialyzed AgNP–CNF samples respectively. The results showed a significant growth inhibition when an undialyzed CNF–AgNP sample was used (ESI, Fig. S2†), whereas the dialyzed CNF–AgNPs at the same concentration did not inhibit bacterial growth. Thus, this study further highlighted the importance of sample purification, and the critical need to remove the excess Ag^+ precursors and/or unbound AgNPs to avoid an overestimation of the antibacterial properties of the nanocomposite material. To the best of our knowledge, prior studies have not evaluated the role of the precursor material or free AgNPs on the antibacterial properties of silver nanocomposite materials. In addition to the above factors, the attachment of AgNPs on a large support such as CNFs may also impeded the diffusion and release of Ag^+, hence limiting the microbial–material interactions as compared to free colloidal AgNPs.

CNF–AgNPs induce production of extracellular polysaccharide-like material around bacteria

The dynamic interactions between bacteria, CNFs and CNF–AgNPs were also observed using fluorescence microscopy and TEM imaging (Fig. 7). From the fluorescence images (acquired using a 10× objective), the bacteria appeared individually suspended in the control sample (Fig. 7A), whereas a few strands of bacteria were seen when incubated with CNFs (Fig. 7B, arrows). When incubated with 150 μM CNF–AgNPs, clusters of bacteria were observed in the fluorescence image (Fig. 7C, arrows). On the other hand, no bacterial cells could be seen when bacteria were incubated with 450 μM CNF–AgNPs (Fig. 7D). Instead small, individual dark spots were observed throughout the image (Fig 7D), suggesting significant cell lysis and the clustering of AgNPs in the presence of bacteria at the higher concentration (Fig. 7D, inset).

The morphology of a single bacterium from each sample was further examined using TEM (Fig. 7E–H). The control bacterium had a characteristic rod-shaped structure of *E. coli* with intact cell walls (Fig. 7E). When incubated with CNFs, a fibrous layer resembling extracellular polysaccharides (EPS) was observed surrounding the bacterium (Fig. 7F). This EPS-like structure was also observed on the bacterium with 150 μM CNF–AgNPs, but the EPS-like structure was more extensive compared to that of the CNF sample (Fig. 7G). Moreover, the production of an EPS-like structure also resulted in the clustering of neighbouring bacteria in solution (ESI, Fig. S3†). However, due to the density of the EPS-like structure, it was unclear from the TEM images if the CNF (Fig. 7F) and CNF–AgNPs (Fig. 7G) were embedded within the EPS-like structure or remained unattached. In contrast, individual AgNPs were seen attached to the surface of the bacterium when a higher concentration of CNF–AgNPs (450 μM) was used (Fig. 7H). It has been suggested that the interaction between AgNPs and the negatively charged groups on the bacterial cell wall[34] could lead to subsequent membrane perforation and cell lysis.[3,34]

To further confirm the antibacterial mechanism of the CNF–AgNPs, fluorescence microscopy analysis using a membrane impermeable dye, propidium iodide (PI), was carried out (ESI, Fig. S4†). From the fluorescence images, the bacteria + CNF samples showed only a few PI-labeled bacteria (ESI, Fig. S4A†), suggesting that the CNF alone did not cause significant bacterial membrane damage. On the other hand, when incubated with 450 μM CNF–AgNPs (ESI, Fig. S4B†), a large population of bacteria in the sample was aggregated and labeled with the PI dye. This indicated that substantial bacterial cell wall and membrane damage could be caused by a high dosage of CNF–AgNPs. The antibacterial mechanism of the CNF–AgNP is likely driven by the initial attachment of AgNPs to

Table 3 Cell viability and bacterial colony count after 18 h of incubation with CNFs or CNF–AgNPs (150 and 450 μM) at 37 °C. The absorbance of reduced MTT precipitate was measured at 560 nm and normalized to the control cells. MTT data represent mean ± SD, $N = 3$. *P*-values were compared to the control

Sample	Cell viability (mean ± SD, *p*-value)	Colony count (CFU mL^{-1})
Control	1.0 ± 0.0	2.7×10^9
CNFs	1.1 ± 0.1 ($p > 0.05$)	2.0×10^9
CNG–AgNPs (150 μM)	1.0 ± 0.1 ($p > 0.05$)	3.6×10^8
CNF–AgNPs (450 μM)	0.6 ± 0.2 ($p < 0.001$)	2.1×10^6

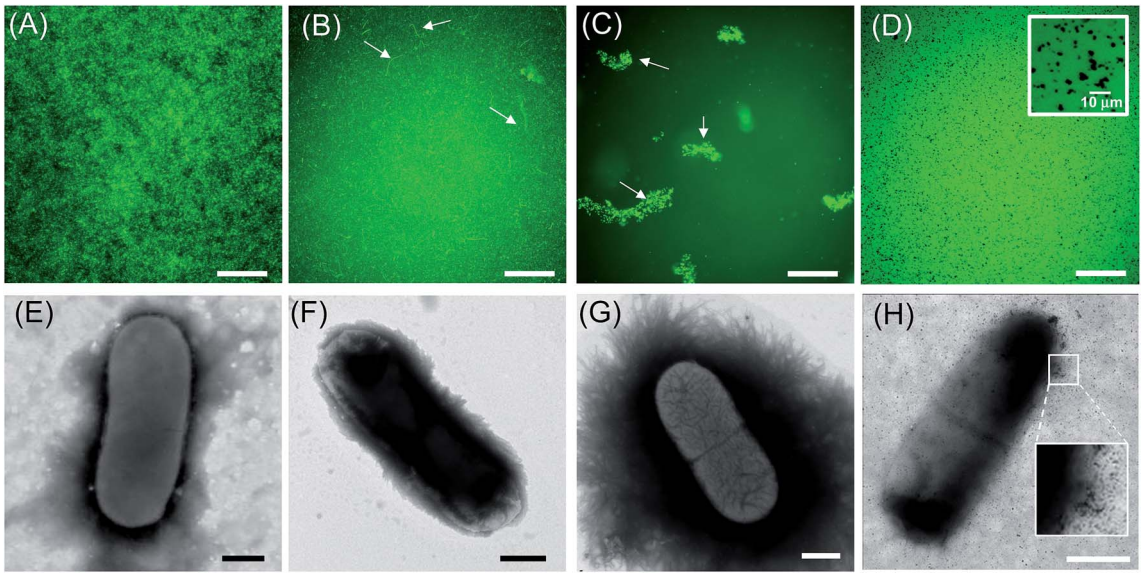

Fig. 7 Structural analyses of bacterial suspension by fluorescence microscopy and TEM imaging. Fluorescence microscopy images of bacteria in the (A) control and after incubation with (B) 0.008% CNF, (C) 150 μM and (D) 450 μM CNF–AgNPs for 18 h at 37 °C. Scale bars on the fluorescence images = 100 μm. Representative TEM images of the (E) control bacteria, (F) bacteria with 0.008% CNF, and bacteria incubated with (G) 150 μM and (H) 450 μM CNF–AgNPs for 18 h at 37 °C. Scale bars on the TEM images = 500 nm.

the bacterial cell surface (Fig. 7H), followed by the interaction of AgNPs and Ag^+ with the bacterial cell wall, which caused damage to the bacterial cell wall and perforation of the cell membrane (ESI, Fig. S4†). Consequently, the damage caused by AgNPs and Ag^+ to the bacterial cell wall and membrane resulted in a growth inhibition (Fig. 6), decrease in bacterial viability and cell count (Table 1), and eventual lysis of bacterial cell, as indicated by a lack of bacterial cells in the fluorescence image (Fig. 7D) compared to the control sample.

At a sub-lethal concentration of CNF–AgNPs, however, an EPS-like structure was seen surrounding the bacterium (Fig. 7F–G). Bacterial EPS production is a widespread phenomenon in bacterial biofilms.[35,36] One of the unique properties of EPS is its ability to form complex with metal ions, such as cadmium, chromium, lead, molybdenum, nickel and molybdenum.[35,36] The ability of EPS to complex and remove metal ions from its surrounding is believed to be an innate defense mechanism of bacteria against toxic environmental stress such as oxidation.[37] Whether the CNF–AgNP has a causal role in inducing the production of bacterial EPS and the exact biochemical synthesis of CNF–AgNPs induced EPS production remain to be elucidated, but it is beyond the scope of this study.

Conclusions

CNF–AgNPs were synthesized by electrostatic binding of Ag^+ on negatively charged CNF surfaces, followed by the reduction to atomic silver and AgNPs on CNFs. The results of this study showed that the CNF was an excellent dispersing agent for AgNPs. At 150 μM equivalent Ag^+ concentration, CNF–AgNPs induced the production of an EPS-like material, causing clustering of bacteria in solution. However, at high CNF–AgNP concentration, a significant decrease in bacterial growth, viability and count was observed. The ability of CNF–AgNPs to induce bacterial EPS production and aggregate bacteria could be of significant interest for diverse applications, including bio-fermentation, antibacterial packaging, wound dressings and bio-separation of microbes from complex soil and food materials.

Acknowledgements

This work was supported by the AFRI Grant (2011-67021-20034) from the USDA-NIFA.

References

1 H. S. Barud, T. Regiani, R. F. C. Marques, W. R. Lustri, Y. Messaddeq and S. J. L. Ribeiro, *J. Nanomater.*, 2011, DOI: 10.1155/2011/721631.
2 Q. L. Feng, J. Wu, G. Q. Chen, F. Z. Cui, T. N. Kim and J. O. Kim, *J. Biomed. Mater. Res.*, 2000, **52**, 662–668.
3 I. Sondi and B. Salopek-Sondi, *J. Colloid Interface Sci.*, 2004, **275**, 177–182.
4 J. R. Morones, J. L. Elechiguerra, A. Camacho, K. Holt, J. B. Kouri, J. T. Ramirez and M. J. Yacaman, *Nanotechnology*, 2005, **16**, 2346–2353.
5 T. Maneerung, S. Tokura and R. Rujiravanit, *Carbohydr. Polym.*, 2008, **72**, 43–51.
6 J.-S. Lee, A. K. Lytton-Jean, S. J. Hurst and C. A. Mirkin, *Nano Lett.*, 2007, **7**, 2112–2115.
7 X. Li and J. J. Lenhart, *Environ. Sci. Technol.*, 2012, **46**, 5378–5386.
8 M. Rai, A. Yadav and A. Gade, *Biotechnol. Adv.*, 2009, **27**, 76–83.

9 G. Martinez-Castanon, N. Nino-Martinez, F. Martinez-Gutierrez, J. Martinez-Mendoza and F. Ruiz, *J. Nanopart. Res.*, 2008, **10**, 1343–1348.
10 D. Wei, W. Sun, W. Qian, Y. Ye and X. Ma, *Carbohydr. Res.*, 2009, **344**, 2375–2382.
11 P. Raveendran, J. Fu and S. L. Wallen, *J. Am. Chem. Soc.*, 2003, **125**, 13940–13941.
12 I. Diez, P. Eronen, M. Osterberg, M. B. Linder, O. Ikkala and R. H. A. Ras, *Macromol. Biosci.*, 2011, **11**, 1185–1191.
13 H. Dong, J. F. Snyder, D. T. Tran and J. L. Leadore, *Carbohydr. Polym.*, 2013, **95**, 760–767.
14 N. Drogat, R. Granet, V. Sol, A. Memmi, N. Saad, C. K. Koerkamp, P. Bressollier and P. Krausz, *J. Nanopart. Res.*, 2011, **13**, 1557–1562.
15 J. George, V. A. Sajeevkumar, K. V. Ramana, S. N. Sabapathy and Siddaramaiah, *J. Mater. Chem.*, 2012, **22**, 22433–22439.
16 S. Padalkar, J. R. Capadona, S. J. Rowan, C. Weder, Y.-H. Won, L. A. Stanciu and R. J. Moon, *Langmuir*, 2010, **26**, 8497–8502.
17 R. Xiong, C. H. Lu, W. Zhang, Z. H. Zhou and X. X. Zhang, *Carbohydr. Polym.*, 2013, **95**, 214–219.
18 H. Liu, D. Wang, Z. Song and S. Shang, *Cellulose*, 2011, **18**, 67–74.
19 H. Liu, J. Song, S. B. Shang, Z. Q. Song and D. Wang, *ACS Appl. Mater. Interfaces*, 2012, **4**, 2413–2419.
20 A. R. Lokanathan, K. M. A. Uddin, O. J. Rojas and J. Laine, *Biomacromolecules*, 2014, **15**, 373–379.
21 S. Ifuku, M. Tsuji, M. Morimoto, H. Saimoto and H. Yano, *Biomacromolecules*, 2009, **10**, 2714–2717.
22 C. Aymonier, U. Schlotterbeck, L. Antonietti, P. Zacharias, R. Thomann, J. C. Tiller and S. Mecking, *Chem. Commun.*, 2002, 3018–3019.
23 M. C. Rodríguez-Argüelles, C. Sieiro, R. Cao and L. Nasi, *J. Colloid Interface Sci.*, 2011, **364**, 80–84.
24 W. R. Li, X. B. Xie, Q. S. Shi, H. Y. Zeng, Y. S. Ou-Yang and Y. B. Chen, *Appl. Microbiol. Biotechnol.*, 2010, **85**, 1115–1122.
25 Y. Cheng, L. Yin, S. Lin, M. Wiesner, E. Bernhardt and J. Liu, *J. Phys. Chem. C*, 2011, **115**, 4425–4432.
26 P. Lu and Y. L. Hsieh, *Carbohydr. Polym.*, 2012, **87**, 564–573.
27 F. Jiang and Y.-L. Hsieh, *Carbohydr. Polym.*, 2013, **95**, 32–40.
28 F. Jiang, S. Han and Y.-L. Hsieh, *RSC Adv.*, 2013, **3**, 12366–12375.
29 Y. Fang, *J. Chem. Phys.*, 1998, **108**, 4315–4318.
30 F. Jiang, L. J. Dallas, B. K. Ahn and Y.-L. Hsieh, *Carbohydr. Polym.*, 2014, **110**, 360–366.
31 N. Akthar, S. Sastry and M. Mohan, *Biotechnol. Lett.*, 1995, **17**, 551–556.
32 S. M. Heard, F. Grieser, C. G. Barraclough and J. V. Sanders, *J. Colloid Interface Sci.*, 1983, **93**, 545–555.
33 L. Kvitek, A. Panáček, J. Soukupova, M. Kolar, R. Vecerova, R. Prucek, M. Holecová and R. Zboril, *J. Phys. Chem. C*, 2008, **112**, 5825–5834.
34 S. Shrivastava, T. Bera, A. Roy, G. Singh, P. Ramachandrarao and D. Dash, *Nanotechnology*, 2007, **18**, 225103.
35 I. Beech and C. S. Cheung, *Int. Biodeterior. Biodegrad.*, 1995, **35**, 59–72.
36 G. Guibaud, S. Comte, F. Bordas, S. Dupuy and M. Baudu, *Chemosphere*, 2005, **59**, 629–638.
37 D. Pan and X. Mei, *Carbohydr. Polym.*, 2010, **80**, 908–914.